Benthic biogeochemical processes and fluxes in the hypoxic and acidified northern Gulf of Mexico (nGoM), part I: Carbonate dissolution from in situ microprofiles

Eva Ferreira, Bruno Lansard, Gaël Monvoisin, Evan Magette, Anthony Boever, Hanna Bridgham, Bruno Bombled, Jordon Scott Beckler, Martial Taillefert, Christophe Rabouille

Marine Chemistry 270 (2025) 104515

Contents lists available at ScienceDirect

Marine Chemistry

journal homepage: www.elsevier.com/locate/marchem

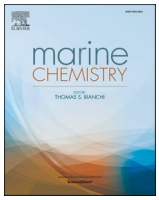

Benthic biogeochemical processes and fluxes in the hypoxic and acidified northern Gulf of Mexico (nGoM), part I: Carbonate dissolution from *in situ* microprofiles

Eva Ferreira [a,*], Bruno Lansard [a], Gaël Monvoisin [b], Evan Magette [c], Anthony Boever [c], Hanna Bridgham [d], Bruno Bombled [a], Jordon Scott Beckler [d], Martial Taillefert [c], Christophe Rabouille [a]

[a] LSCE, Laboratoire des Sciences du Climat et de l'Environnement, UMR 8212: CEA-CNRS-UVSQ-UPSaclay and IPSL, F-91198 Gif-sur-Yvette, France
[b] GEOPS-Geosciences Paris-Saclay, UMR 8148: UPSaclay-CNRS and IPSL, F-91405 Orsay, France
[c] Georgia Institute of Technology, School of Earth and Atmospheric Sciences, Atlanta, GA 30332, United States of America
[d] Harbor Branch Oceanographic Institute, Florida Atlantic University, Fort Pierce, FL 34946, United States of America

ARTICLE INFO

Keywords:
Surface sediment
Coastal ocean
Eutrophication
Calcium
Carbonate system
Acidification
Hypoxia

ABSTRACT

The northern Gulf of Mexico (nGoM) experiences seasonal coastal hypoxia due to nutrient enrichment from the Mississippi-Atchafalaya River basin, leading to one of the world's largest hypoxic zones. In these shallow zones, benthic processes play an essential role in driving/maintaining deoxygenation and acidification of bottom waters. In this regard, this paper investigates carbonate dissolution processes in surface sediment of the nGoM during hypoxic conditions in summer 2022, as the main acidification feedback mechanism, with a specific focus on the effects of bottom water acidification. A strong linear relationship is observed between oxygen and pH, with a pH difference of 0.37 between the most oxygenated and the nearly anoxic station, reaching a value of 7.63. Using high-resolution techniques, this study combines pH and O_2 microprofiling (200 μm) with benthic measurements of carbonate system parameters (pH, DIC, TA, Ca^{2+}) to assess carbonate dissolution at millimeter-scale resolution. The pH microprofiles reveal a significant decrease in the first 3 cm, with pore water pH reaching values of 6.90 at the most hypoxic station. Despite undersaturation with respect to aragonite and occasionally calcite, Ca^{2+} profiles indicate no significant carbonate dissolution, suggesting stability of calcium carbonate in these sediments during the summer. This lack of dissolution, likely influenced by the absence of aragonite, and possible inhibitory effects of dissolved organic carbon and orthophosphate, points to a limited buffering capacity in these sediments. These insights are essential for refining models predicting coastal acidification and hypoxia responses to environmental stressors in the nGoM and similar eutrophic systems.

1. Introduction

Coastal regions experience various anthropogenic and natural perturbations, altering biogeochemical processes and causing significant environmental changes (Doney, 2010; Bauer et al., 2013). This is especially obvious in densely populated river-dominated ocean margins (RiOMars, McKee et al., 2004; Dai et al., 2022), where riverine inputs constitute additional stressors by inducing excessive nutrient loading (Paerl, 2006) and providing large inputs of terrestrial carbon to the coastal ocean (Bianchi et al., 2007). The input of organic matter (OM) by direct discharge increases oxygen consumption by microbial respiration, leading in some cases to severe hypoxia (Breitburg et al., 2018). The mineralization of OM produces metabolic CO_2, which contributes to the production of dissolved inorganic carbon (DIC) and the decrease in pH of bottom waters (Cai et al., 2011; Wallace et al., 2014). Fluxes of DIC from the sediments to the bottom waters may exacerbate this acidification (Hu et al., 2017; Yin et al., 2024), whereas anoxic mineralization processes may represent sources of total alkalinity (TA) and thus have a buffering effect, producing negative feedback to bottom water acidification (Hu and Cai, 2011). These coastal zones hold significant socio-economic importance (*e.g.* fishing, aquaculture…). However, several studies have shown that eutrophication and deoxygenation can severely

* Corresponding author.
E-mail address: eva.ferreira@lsce.ipsl.fr (E. Ferreira).

https://doi.org/10.1016/j.marchem.2025.104515
Received 7 November 2024; Received in revised form 26 March 2025; Accepted 27 March 2025
Available online 1 April 2025

impact ecosystem health by disrupting the structure of the food chain (Rabalais and Turner, 2019; Doney et al., 2020). In this regard, coastal ocean acidification is an additional stressor as it may disrupt the equilibrium of calcium carbonate ($CaCO_3$) compounds and promote the dissolution of many invertebrate shells (Byrne and Fitzer, 2019). The increase in atmospheric CO_2 inputs to the surface waters increases total DIC, lowers the pH of seawater, and reduce the saturation state (Ω, Eq. 1) of $CaCO_3$ minerals (Doney et al., 2009; Cai et al., 2021), including aragonite (Ω_{Ar}) and calcite (Ω_{Ca}).

$$\Omega = \frac{\left(\left[Ca^{2+}\right] \times \left[CO_3^{2-}\right]\right)}{K_{sp}^*} \quad (1)$$

where $[Ca^{2+}]$ and $[CO_3^{2-}]$ are the dissolved calcium and carbonate ions activities and K_{sp}^* is the apparent solubility equilibrium constant of each carbonate polymorph, *i.e.* aragonite and calcite (Mucci, 1983).

Total alkalinity fluxes across the sediment-water interface (SWI) are regulated by diagenetic processes and play a critical role in maintaining bottom water pH conditions, especially in estuarine and coastal ocean environments hosting organic-rich sediments (Magette et al., in prep; Krumins et al., 2013; Rassmann et al., 2020; Yin et al., 2024). In this context, the dissolution of sedimentary carbonates may play a key role in buffering the pH of coastal waters (Mucci et al., 2000; Jahnke and Jahnke, 2004; Rao et al., 2014), as it generates 2 mol of TA and 1 mol of DIC. Current models estimate carbonate dissolution about 7 Tmol yr^{-1} in shallow sediments resulting in a net alkalinity flux of 13.3 Teq yr^{-1} (Krumins et al., 2013). Despite the increasing risk of coastal ocean acidification in the near future, the potential for the dissolution of calcium carbonates in shallow waters and the magnitude of the negative feedback on acidification remain key unknowns to address in RiOMar systems (Cai et al., 2021).

The Louisiana shelf, located in the northern Gulf of Mexico (nGoM), is heavily impacted by nutrient inputs from the Mississippi-Atchafalaya River basin. This area is known for its severe and recurrent hypoxic crises in summer (Rabalais et al., 2002), which lead to seasonally-enhanced acidification of the bottom waters (Turner et al., 2008; Cai et al., 2011; Laurent et al., 2017; Jiang et al., 2019; Rabouille et al., 2021). These conditions are favorable to carbonate dissolution, especially in the sediment where $CaCO_3$ undersaturation conditions can be reached in response to intense early diagenetic reactions. Earlier studies, have questioned the extent of $CaCO_3$ dissolution based on DIC and TA benthic fluxes (Berelson et al., 2019), and reported calcite and aragonite undersaturation ($\Omega < 1$) in surface sediments, suggesting carbonate dissolution (Rabouille et al., 2021). However, the question remains unresolved in cases of extreme acidification, where undersaturation could be reached, especially in this area during the summer period, when bottom water pH reduction is important in response to hypoxia. Previous studies lacked the vertical resolution to accurately measure dissolved calcium concentrations near the SWI and fully elucidate this process. In fact, few studies on a global scale have been able to quantify or unequivocally observe carbonate dissolution in the sedimentary column, let alone in the nGoM area, due to technical limitations associated with calcium measurements and the needs for a high spatial resolution.

This study addresses these gaps by employing high vertical resolution techniques for pore water extraction and *in situ* measurements of O_2 and pH microprofiles. Using these techniques, the distribution of the carbonate system parameters (pH, DIC, TA, and Ca^{2+}) was determined at a millimeter-scale resolution in pore waters along an east-west transect in the nGoM during the summer of 2022. The effect of bottom water acidification on carbonate dissolution in surficial sediments was examined, along with potential mitigating factors. These findings ultimately contribute to a comprehensive understanding of coastal carbon cycling dynamics and will benefit to future studies, as various projections suggest that acidification will increase in the coming decades due to rising atmospheric CO_2 and ongoing eutrophication (Cai et al., 2011).

2. Materials and methods

2.1. Study site

In July 2022, a sampling cruise was conducted in the nGoM aboard the R/V Savannah (Skidaway Institute of Oceanography, University of Georgia), part of a cycle of five seasonal cruises between 2020 and 2022. This study focuses on a 180 km long transect along the Louisiana shelf (Fig. 1), including seven stations (Table 1) with depth ranging from 14 to 90 m. The annual report concerning shelf wide hypoxia for the summer of 2022 indicates a "Dead Zone" extension of 8480 km^2 (Rabalais, 2022), defined by areas with O_2 concentrations below the hypoxic limit of 63 μmol L^{-1} (Rabalais and Turner, 2001). The stations located in the western part of the transect, stations MK, 4, and 5b, fall within a zone with a 50 to 100 % chance of experiencing hypoxia each summer (Rabalais and Turner, 2019). These stations were examined in a previous campaign in Summer 2017, during which *in situ* pH and O_2 microprofiles as well as *ex situ* profiles of TA, DIC, SO_4^{2-}, NO_3^-, NH_4^+, $\sum PO_4^{3-}$, dissolved Mn, dissolved Fe(II), and Fe(III) were obtained (Rabouille et al., 2021).

2.2. Bottom water and overlying water measurements

Seawater samples were collected using a rosette with 10 × 6 L Niskin bottles. The rosette was equipped with a conductivity-temperature-depth sensor (CTD, Seabird SBE-19), a dissolved oxygen sensor (Seabird, SBE 43), a turbidity sensor (ECO-BB, Wet Lab), and a fluorometer (Seapoint). All sensors were calibrated by the manufacturers before the cruise. In addition to the vertical oxygen profiles measured by the CTD's sensor in the water column, discrete oxygen measurements were carried out in surface, intermediate, and bottom waters by Winkler titration (Hansen, 1999) immediately after sampling. Bottom water samples were collected with the deepest Niskin bottle, as close as possible to the seafloor (*i.e.* 1–3 m above the sediment). The winch payload weight was monitored to ensure impact with the seafloor did not occur. The Apparent Oxygen Utilization (AOU, Eq. (2)) was calculated as the difference between the saturated concentration of oxygen, determined from temperature and salinity (Murray and Riley, 1969) and the measured oxygen concentration.

$$AOU = O_{2,sat} - O_{2,obs} \quad (2)$$

Due to the steep gradients observed a few meters above the seafloor in the CTD profiles (Appendix 1) and noted in previous studies (Rabouille et al., 2021), we used the oxygen concentrations measured by an optode deployed simultaneously on a separate benthic chamber (Magette et al., in prep) as the overlying water (OW) oxygen concentration ($O_{2\text{-}OW}$). The benthic chamber lander carrying the optode was deployed within 10–15 cm above the sediment-water interface.

To measure TA and DIC, 500 mL of bottom waters were sampled into borosilicate bottles, poisoned with 100 μL of supersaturated $HgCl_2$, and stored in the dark at 4 °C. The SNAPO-CO2 Service facilities (LOCEAN, Paris, France) conducted measurements by potentiometric titration using a closed-cell titration protocol (DOE, 1994; Metzl et al., 2024). The CRMs provided by Dr. A. Dickson (Batch 204, Scripps Institution of Oceanography, San Diego, USA) were used to calibrate the measurement with a respective accuracy of ±0.11 % and 0.21 % for TA and DIC. The pH of bottom waters was determined on board by the spectrophotometric method with purified m-cresol purple after temperature stabilization within a few hours of sampling at 25 °C (Clayton and Byrne, 1993; Liu et al., 2011). Triplicate measurements were made, and the overall precision was better than ±0.003 pH units. The *in situ* pH was then recalculated at *in situ* pressure and temperature conditions with the CO2SYS program (Pierrot et al., 2006) using the dissociation constants K_{a1} and K_{a2} from Lueker et al. (2000), $KHSO_4$ reported by Dickson (1990) and total dissolved boron reported by Uppström (1974) following the recommendations by Orr et al. (2015). The *in situ* pH is reported on the total proton scale (pH_T). The obtained *in situ* pH_T was

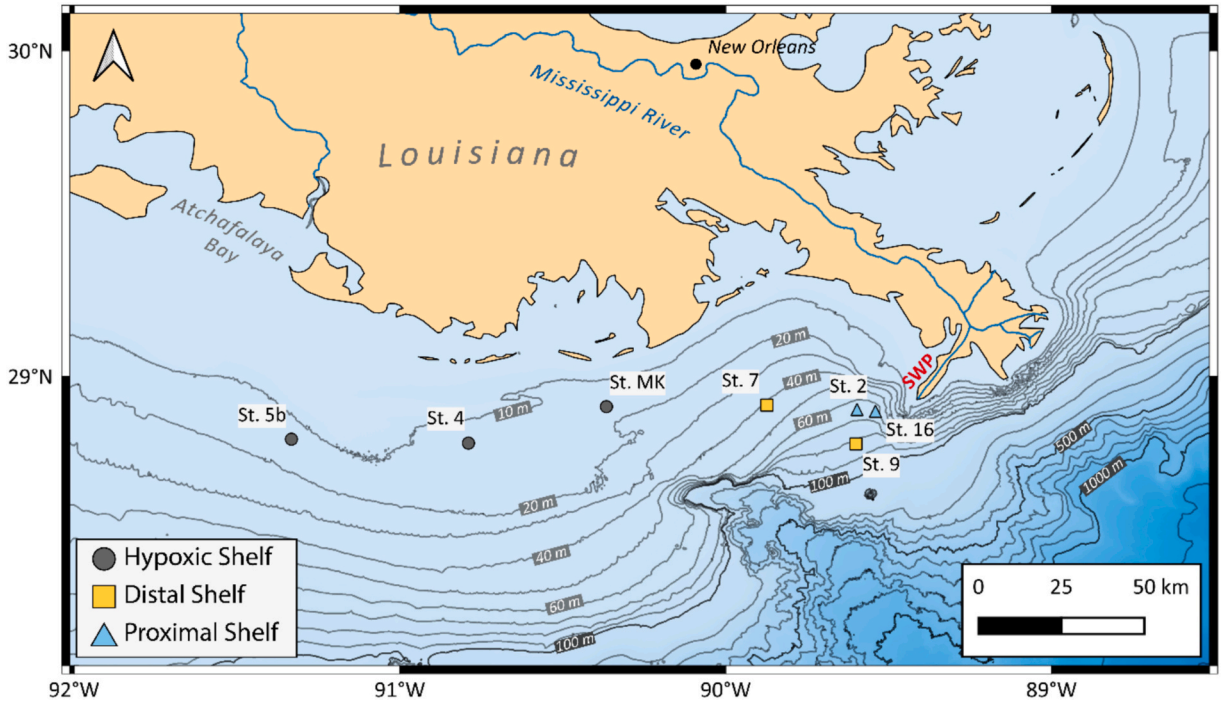

Fig. 1. Map of the Louisiana shelf showing the location of the stations sampled by the R/V Savannah in July 2022. Stations are grouped by the following criteria: 1) Hypoxic shelf (HS, grey circles) on the shelf which experience bottom water hypoxia during any sampling period; 2) Distal shelf (DS, yellow squares) on the shelf which do not experience hypoxia during any sampling period; and 3) Proximal shelf (PS, blue triangles) at the Mississippi River mouth which do not experience hypoxia. SWP = Southwest pass. NOAA National Centers for Environmental Information (2023). (For interpretation of the references to colour in this figure legend, the reader is referred to the web version of this article.)

Table 1
Position and water depth of the seven sampling stations on the Louisiana shelf in the summer of 2022, along with bottom water (BW) temperature, salinity, O_2, apparent oxygen utilization (AOU), dissolved inorganic carbon (DIC), total alkalinity (TA) and pH recorded at the Niskin depth.

St.	Date (DD/MM/YY)	Latitude (°N)	Longitude (°W)	Water Depth (m)	Niskin Depth (m)	BW Temp. (°C)	BW Sal.	BW O_2 (μmol L^{-1})	BW AOU (μmol L^{-1})	BW DIC (μmol kg^{-1})	BW TA (μmol kg^{-1})	BW pH_T
5b	10/07/22	28°47′52.4	91°19′19.8	14	11	27.4	35.0	24.4	178.5	2233	2358	7.634
4	09/07/22	28°47′35.4	90°41′50.7	20	17	27.5	35.5	68.8	133.2	2200	2375	7.742
MK	11/07/22	28°54′11.0	90°18′03.9	20	17	25.7	36.0	78.0	129.2	2197	2388	7.799
7	12/07/22	28°54′33.5	89°51′26.7	42	41	24.3	36.3	53.7	158.5	2227	2382	7.737
9	16/07/22	28°47′09.8	89°35′53.2	83	80	19.2	36.5	122.6	109.6	2188	2391	7.913
2	17/07/22	28°53′48.1	89°35′12.7	64	62	22.2	36.5	182.8	58.1	2131	2404	8.001
16	20/07/22	28°53′31.3	89°32′17.0	60	57	23.0	36.3	158.8	36.8	2154	2412	7.961

compared to the pH value computed using measured DIC and TA (SNAPO-CO2) at *in situ* conditions with the same parameters. These two independent values were in good agreement within 0.01 pH units or better.

2.3. Sediment sampling and characterization

Sediment samples were collected using a multi-corer (MC-800, Ocean Instrument). Cores with the best-preserved SWI were selected for pore water extraction. Cores were extruded in a glove box under an oxygen-free environment (purged with N_2). Sediment porosity was determined separately by dehydrating approximately 1–2 g of the various section at 60 °C for more than 24 h, adjusting for the residual mass of salt. Sediment volume was estimated assuming a density of dry sediment of 2.65 g cm^{-3}, whereas water volume was derived from the mass of evaporated water. The particulate inorganic carbon (PIC) content of the sediment was obtained by weighing dry sediment before and after removing inorganic carbon *via* dissolution in 1 % hydrochloric acid (HCl) to obtain the percentage of carbonate by mass loss. The identification of $CaCO_3$ polymorphs (*i.e.* aragonite and calcite) was performed by X-ray micro-diffraction with a Bruker D8 Advance. A calibration range was made from a mixture of pure aragonite coral reduced in powder and pure calcite (Specpure, Batch S95458). The chosen measurement range focused on carbonates (aragonite and calcite) with angles between 25 and 32°2θ at 40 Kev and 30 mA with an Eiger2R_R500K detector in 1D integration mode.

2.4. Sediment pore water extraction and analyses

Sediment pore waters were extracted within one hour of collection from two additional cores with a well-preserved interface. To quantify the distribution of DIC and TA in sediment pore waters, the core was sliced into 0.7–5 cm thick sections, depending on depth, in a glove bag under N_2 atmosphere to maintain anoxic conditions. Then pore waters were extracted by centrifugation and filtered through 0.2 μm filters, both under N_2 atmosphere, poisoned with 10 μL of saturated $HgCl_2$, and

stored in 2 mL glass vials at 4 °C until analysis. DIC measurements were performed on 0.75 mL using a cavity ring-down spectrometry (CRDS, Picarro G2131-i) using an automatic CO_2 extraction system (Apollo SciTech AS-D1) with a 10 mL injection syringe (Deng et al., 2022). The instrument was calibrated with seawater reference material, CRMs supplied by the Scripps Institution of Oceanography (University of California, San Diego) with certified DIC and TA concentrations (Batch 199). The relative uncertainty for DIC was ±0.5 %. TA measurements were carried out on 0.75 mL pore water aliquots by open-cell potentiometric titration (SOP3b, Dickson et al., 2007) using HCl (0.005 M) as titrant. The acid was calibrated in triplicate before and after each series of measurements using the same seawater reference material used for the DIC analyses. The relative uncertainty for the TA measurements was ±0.5 %. A second core was used for the pore water extractions to improve the spatial resolution of the calcium measurements over the first five centimeters below the SWI. Sections were centrifuged to separate the solid and liquid phases, and 2 mL volumes were subsampled, acidified (HNO_3 0.005 N), and stored in Eppendorf tubes at 4 °C until analysis. Concentrations of Ca^{2+} were analyzed on 25 µL aliquots (previously diluted by a factor of 200) with a liquid phase ion chromatography system (ICS 1000 *Dionex*™) with CGA6 precolumn, CS16 column and CRDS-600 88 Ma suppressor, following the method described by He et al. (2020). The eluent consisted of 1-Heptane Sulfonic Acid Sodium Salt (HMSA) at a concentration of 15 µmol L^{-1} and delivered with a flow rate of 1.0 mL min^{-1}. The standards were made from IAPSO seawater diluted between 100 and 600 folds, with a relative uncertainty of ±0.5 %.

2.5. *In situ measurements of pH and dissolved oxygen at the sediment water-interface*

A benthic microprofiler (Unisense®) was deployed to measure high-precision pH and dissolved oxygen profiles at the SWI, in the first three centimeters of sediment with a vertical resolution of 200 µm (Rassmann et al., 2016; Rassmann et al., 2020; Rabouille et al., 2021 and references therein). The profiler was equipped with five Clark Au/Ag microelectrodes for oxygen measurements (Revsbech, 1989), two glass microelectrodes for pH measurements, two Ag/AgCl pH reference electrodes and a miniaturized resistivity probe. The O_2 microelectrodes were calibrated using a two-point calibration technique, response to variation in oxygen concentrations being linear (Boudreau and Jorgensen, 2001). The $O_{2\text{-}OW}$ values from the benthic chamber optode were used to calibrate the oxygen microprofiles. The microelectrode's signal in the anoxic part of the pore waters was used to set readings to 0 µmol L^{-1}. The oxygen penetration depth (OPD), defined as the depth where the O_2 concentrations drop below 1 µmol L^{-1} into the sediment (Rabouille and Gaillard, 1991), was determined using the *in situ* microelectrode profiles. Diffusive oxygen uptake rates (DOU) were calculated using Fick's first law (Eq. 3, Berner, 1980).

$$\mathrm{DOU} = -D_s \cdot \varphi \cdot \left.\frac{\mathrm{d}[O_2]}{\mathrm{dz}}\right|_{z=0} \quad (3)$$

Where D_s is the apparent diffusion coefficient of O_2 corrected for sediment tortuosity at *in situ* temperature (Li and Gregory, 1974; Glud, 2008), $\left.\frac{\mathrm{d}[O2]}{\mathrm{dz}}\right|_{z=0}$ the O_2 gradient on the first 400 µm below the SWI and φ surface sediment porosity.

The pH microelectrodes were calibrated onboard using NBS buffers (pH 4.00, 7.00, and 10.00 at 25 °C). The microelectrode signal was converted into ΔpH by using the NBS slope recalculated at *in situ* temperature. Subsequently, the pH_T value was calculated using the pH_T of the overlying water (10–15 cm above the sediment) recalculated from the $O_{2\text{-}OW}$ obtained by the optode (see above), and the linear regression between pH_T and O_2 (see below).

2.6. *Calculation of the carbonate saturation state*

The saturation states of seawater, with respect to aragonite (Ω_{AR}) and calcite (Ω_{CA}), were calculated using the CO2SYS program (Pierrot et al., 2006) following the recommendations of Orr et al. (2015). The pH_T and TA measurements, *in situ* bottom water pressure, temperature, and salinity, and dissolved inorganic phosphate and silicate data from Berelson et al. (2019) were used as input parameters. Vertical profiles of Ω at a millimeter scale below the SWI were calculated from *in situ* pH_T microprofiles and linear interpolation of the centimeter-scale TA profiles between each seven points in the first four centimeters (Rabouille et al., 2021).

3. Results

3.1. *Bottom water measurements*

Characteristics of the bottom waters sampled along the oceanographic transect are reported in Table 1. Bottom water mean temperatures were 26.9 °C at the shallowest stations (St. 5b, 4 and MK, hypoxic shelf, Fig. 1) and reached a minimum of 19.2 °C at the deepest station (St. 9). The mean salinity of the transect is 36.0 ± 0.5, with a minimum reached in the hypoxic zone and the maximum in the proximal stations.

From the Mississippi mouth (St. 16) to the Louisiana shelf (St. 5b), a significant increase in DIC concentrations of bottom waters (+ 79 µmol kg^{-1}) was accompanied by a TA decrease (−54 µmol kg^{-1}) (Table 1). The bottom water oxygen concentrations (*i.e.*, from Niskin bottle samples) showed a significant decrease by 159 µmol L^{-1} along the east-west transect, with normoxic bottom water in the proximal zone near the mouth of the Mississippi River, and nearly anoxic bottom waters at station 5b, located at the western end of the transect off Atchafalaya Bay (Table 1). In addition to this spatial gradient along the transect, CTD profiles show strong vertical gradients of decreasing oxygen with depth, particularly pronounced in hypoxic shelf (Appendix 1).

A concomitant decrease in O_2 and pH_T values was observed in bottom waters, contributing to an overall 0.367 pH unit acidification at the most hypoxic station (St. 5b) at the western end of the transect. A strong linear correlation ($r^2 = 0.98$) between oxygen concentrations and pH_T of the bottom waters was observed in both July 2022 and during a previous cruise conducted in July 2017 (Rabouille et al., 2021; Fig. 2).

Considering the strong oxygen gradients observed at the hypoxic stations (St. 5b to 7, Appendix 1), the oxygen optode concentrations obtained in the overlying water 10–15 cm above the sediment (Table 2) were used to process the sediment-water interface data. They obviously showed significantly lower concentrations than these measured in the Niskin bottle, by the CTD-O_2 located 1–3 m above the seabed, with differences reaching up to 63 µmol L^{-1} (Table 2). The vertical oxygen gradients observed at the hypoxic station led to a pronounced hypoxia or near-anoxia at the sediment-water interface whereas this near-bottom gradient was not observed at the normoxic station (St. 9, 16, 2). Following oxygen, the pH_T of the overlying water were recalculated from the linear relationship between the two parameters (Fig. 2). The overlying water pH_T were substantially lower than the bottom water pH_T at the hypoxic stations (Table 2).

3.2. *Sediment characterization, DIC, TA and oxygen in pore waters*

Along the entire transect, surface sediments displayed a homogeneous $CaCO_3$ content, ranging from 10 to 12 % consistent with the conclusions of Balsam and Beeson (2003), with no significant differences between stations (Table 3). The aragonite content of all stations was below the detection limit of the instrument, with no diffraction peaks characteristic of aragonite phases. In turn, the peak of the main form of calcite was observed, suggesting that calcite represents the only form of carbonate minerals in surface sediments.

Generally, the concentrations of DIC and TA in the pore waters

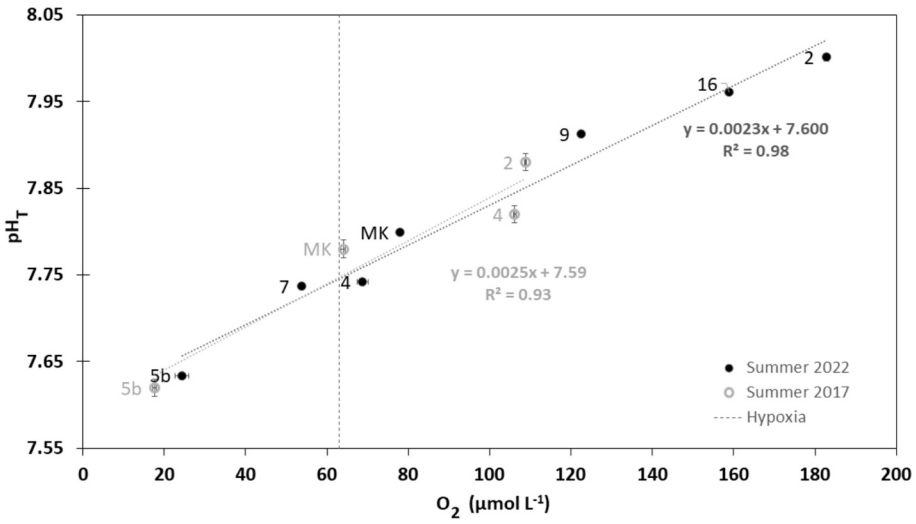

Fig. 2. Bottom water pH_T as a function of bottom water oxygen concentration during the summer 2022 (black circle) and 2017 cruises (grey open circle, Rabouille et al., 2021). When not visible, uncertainties are smaller than the symbol sizes.

Table 2
Overlying water oxygen concentrations ($O_{2\text{-}OW}$) measured by optode and recalculated $pH_{T\text{-}OW}$ (calc. $pH_{T\text{-}OW}$) at the seven sampling stations on the Louisiana shelf in summer 2022. $pH_{T\text{-}OW}$ was calculated by extrapolating the linear regression between O_2 and pH_T (Fig. 2). Difference between BW and OW are calculated in the two last columns. ΔDepth is the depth difference between the deepest Niskin bottle and the optode attached on the benthic chamber as close as possible to the seafloor.

St.	Water Depth	OW O_2	OW pH_T	ΔDepth	ΔO_2 $O_{2\text{-}BW}$-$O_{2\text{-}OW}$	ΔpH $pH_{T\text{-}BW}$-$pH_{T\text{-}OW}$
	(m)	(µmol L^{-1})	(recalc.)	(m)	(µmol L^{-1})	
5b	14	2.3	7.606	3	22.1	0.028
4	20	17	7.640	3	51.8	0.103
MK	20	14.6	7.634	3	63.4	0.165
7	42	45.6	7.705	1	8.1	0.032
9	83	116.1	7.867	3	6.5	0.046
2	64	170.6	7.993	2	12.2	0.008
16	60	184.4	8.025	3	−25.6	−0.064

Table 3
Peak surface area of aragonite and calcite measured by X-ray micro-diffraction and the carbonate content obtained by decarbonation within the top 3.5 cm of sediment at each station.

Station	Depth (cm)	Area Aragonite	Area Calcite	$CaCO_3$ (%)
5b	0.25	0	1851	–
5b	3.50	0	3040	10.2
MK	0.25	0	2150	–
MK	3.50	0	2879	12.7
7	3.50	0	3221	11.9
9	0.25	0	2927	–
9	3.50	0	2491	12.1
2	0.25	0	1707	–
2	3.50	0	1689	12.0
16	0.25	0	1025	–
16	3.50	0	1046	11.2

varied concurrently at the seven stations investigated (Fig. 3). Strong increases of DIC and TA concentrations in pore water were observed across the entire profiles at the stations located near the Mississippi River mouth (St. 2 and 16), with maximum concentrations close to 13,000 µmol kg^{-1} at 35 cm depth at St. 2. In contrast, limited increases

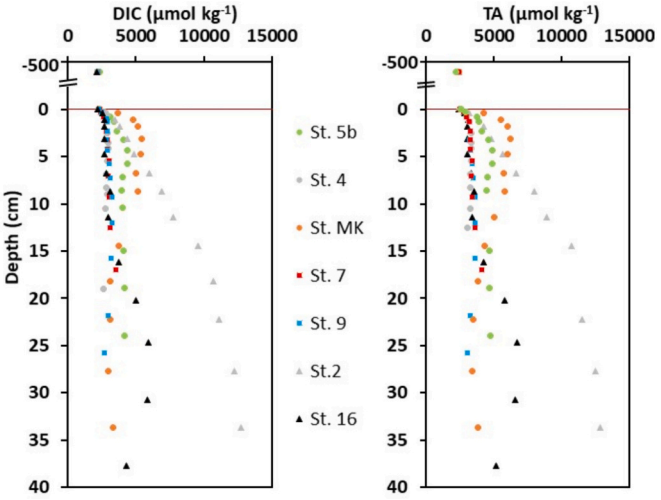

Fig. 3. Pore water profiles of DIC and TA at the seven investigated stations on the Louisiana shelf in July 2022. The red line represents the sediment-water interface (SWI). Uncertainties are smaller than the symbols size. (For interpretation of the references to colour in this figure legend, the reader is referred to the web version of this article.)

in DIC and TA were generally observed within the upper 5 cm of pore waters further on the shelf, and both DIC and TA did not exceed 5000 µmol kg^{-1} at depth.

A net decrease in oxygen concentration was visible below the SWI at all stations, with oxygen penetration proportional to the oxygen content of the overlying waters (Fig. 4). The OPD generally exhibited a decline across the shelf, from ≈1.6 mm at the normoxic proximal stations (St. 2 and 16,) to 0.21 mm at the hypoxic stations (St. MK). At station 5b, the most hypoxic and western station of this study, O_2 concentrations were below the detection limit (data not shown). This observation was consistent with the extremely low concentrations measured with the optode in the overlying waters at this station (Table 2). A gradient in DOU rates was also clearly visible across the shelf, with rates as high as 17.5 mmol m^2 d^{-1} at the most oxygenated stations (St. 2, 16) and close to 0 mmol m^2 d^{-1} at the hypoxic stations (Fig. 4).

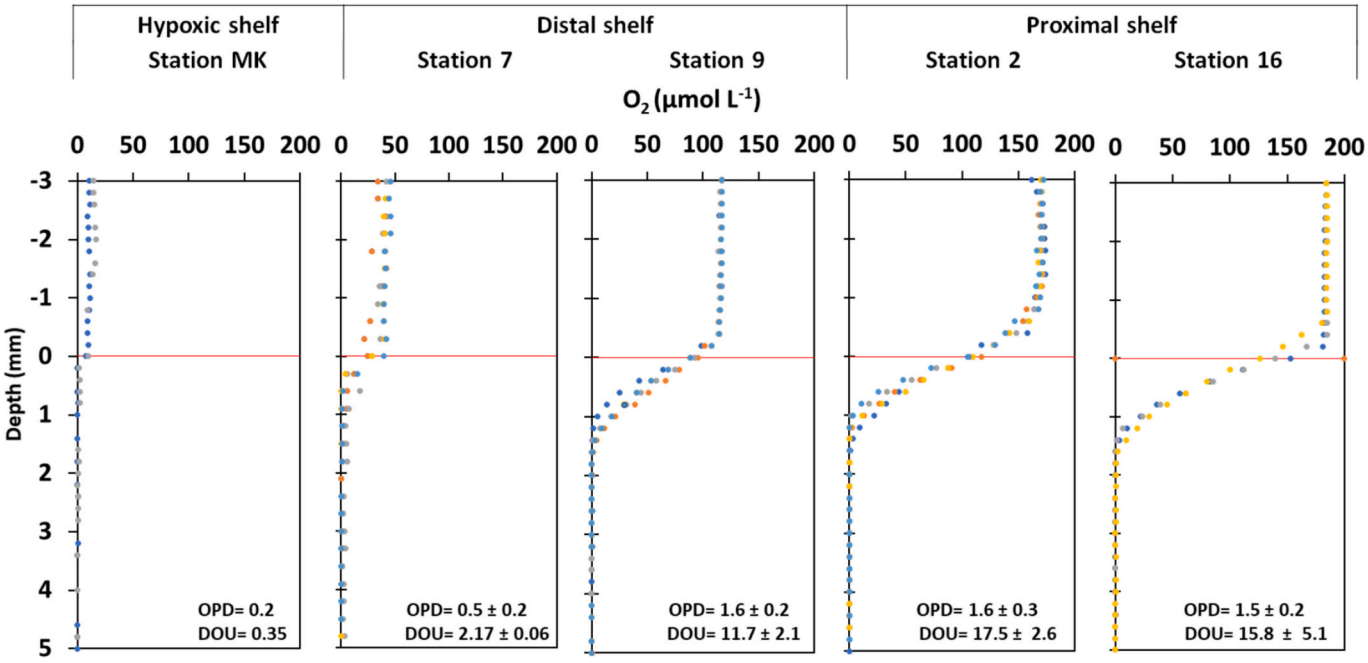

Fig. 4. *In situ* oxygen microprofiles at the sediment-water interface measured on the Louisiana shelf in July 2022. The red line indicates the sediment-water interface. The oxygen penetration depth (OPD, in mm) and the diffusive oxygen uptake rate (DOU, in mmol m^2 d^{-1}) are reported for each station. See text for details. (For interpretation of the references to colour in this figure legend, the reader is referred to the web version of this article.)

3.3. pH, $CaCO_3$ saturation state, and calcium microprofiles in the pore waters

All usable high resolution pH profiles in pore waters revealed a significant pH_T decrease within the first few millimeters below the SWI, followed by various behavior depending on the location along the shelf (Fig. 5a). Closer to the Mississippi River mouth (St. 2, 16, 7, and 9), a pronounced pH decrease was observed in the first few millimeters of the oxic zone that was followed by a rebound in pH of varying intensity depending on the station. The rebound was of approximately 0.2 pH units and spanned depths of around 19 mm at Station 2 and 9, but was much smaller in intensity (0.1 pH unit) and narrower in depth (≈10 mm) at Station 7. At each normoxic station, the pH stabilized around 7.2 to 7.5 at deeper depths. Station 16 showed a different profile compared to the other proximal shelf stations, with a gradual decrease similar to the profiles observed in the hypoxic zone. Indeed, at Station 5b, the pH decreased continuously by approximately 0.7 units to reach a value of 6.90 at 30 mm. Stations 4 and MK exhibited similar profiles with a less pronounced gradient and a final pH near 7.1.

At all stations, overlying waters and sediment pore waters almost entirely displayed oversaturation with respect to calcite and aragonite (Fig. 5b). The saturation state of the overlying waters decreases westward from $\Omega_{Ar} = 3.4$ and $\Omega_{Ca} = 5.2$, at station 16, to $\Omega_{Ar} = 1.6$ and $\Omega_{Ca} = 2.5$ at station 5b. Consistent with the pH_T profiles, saturation states decreased in the thin oxic sediment layer at the proximal stations. Generally, oversaturation with respect to calcite persisted downcore at all stations, except at Station 5b. In contrast, five of the seven stations were slightly undersaturated with respect to aragonite (St. 5b, 4, 7, 9 and 16), with a minimum value of $\Omega_{Ar} = 0.6$ reached at Station 5b.

Dissolved Ca^{2+} concentrations in BW were relatively similar across all stations, ranging from 10.25 mmol L^{-1} (St. 4) to 10.94 mmol L^{-1} (St. 2), consistent with salinity variation and Dittmar's law (data not shown). The vertical distribution of Ca^{2+} concentrations in the pore waters showed no significant variations with depth in the five first centimeters of sediment (Fig. 6). Additionally, no spatially significant differences were observed among the stations; a common average value of 10.22 mmol L^{-1} was measured across all stations, with a standard deviation of 0.21 mmol L^{-1} considering all measurements. On a larger vertical scale (Appendix 2), similar conclusions can be drawn, with little variation in the profiles at each station and no significant differences between stations. The overall average concentration for the extended vertical profiles was 10.15 mmol L^{-1}, with a standard deviation of 0.24 mmol L^{-1} across all measurements.

4. Discussion

4.1. Deoxygenation and acidification of the bottom waters along the east-west shelf transect

The spatial distribution of O_2 concentrations in the bottom and overlying waters reveals large variations in oxygenation of the Louisiana shelf. Indeed, a significant decrease in O_2 concentrations was observed at the shelf stations indicating intense oxygen depletion in the water column that leads to strong hypoxia, as generally observed in July and August (Turner et al., 2008; Rabalais et al., 2002). Three groups of stations can be identified on the basis of their $O_{2\text{-}OW}$ concentrations and their proximity to the Mississippi River (Table 1): proximal stations (PS, St. 2 and 16), distal stations (DS, St. 7 and 9), and hypoxic shelf stations (HS, St. 4, MK and 5b). Stations 2 and 16 displayed normoxic bottom waters even if they are a little bit deeper and on the proximal shelf near the Mississippi River mouth. A decline in bottom water oxygen concentrations followed the east-west transect, with $O_{2\text{-}OW}$ above the threshold for hypoxia (63 µmol L^{-1}) at station 9 (Table 2), but not at station 7 (O_2 < 20 µmol L^{-1}), located westward in shallower waters. Stations MK, 4 and 5b, further to the west, were characterized by acute hypoxia. These low oxygen concentrations have been attributed to the microbial aerobic consumption of labile marine organic matter (Dortch et al., 1994; Bianchi et al., 2010; Turner et al., 2008) originating from primary production in the Mississippi River plume and on the shelf during the spring (Redalje and Fahnenstiel, 1994; Rabalais et al., 2014; Wang et al., 2018). Oxygen consumption occurs both in the water column and in the sediment (Laurent et al., 2016), with sediment contributing to approximately 30 % of the total oxygen consumption in hypoxic layers (Fennel and Testa, 2019). This is supported by the high

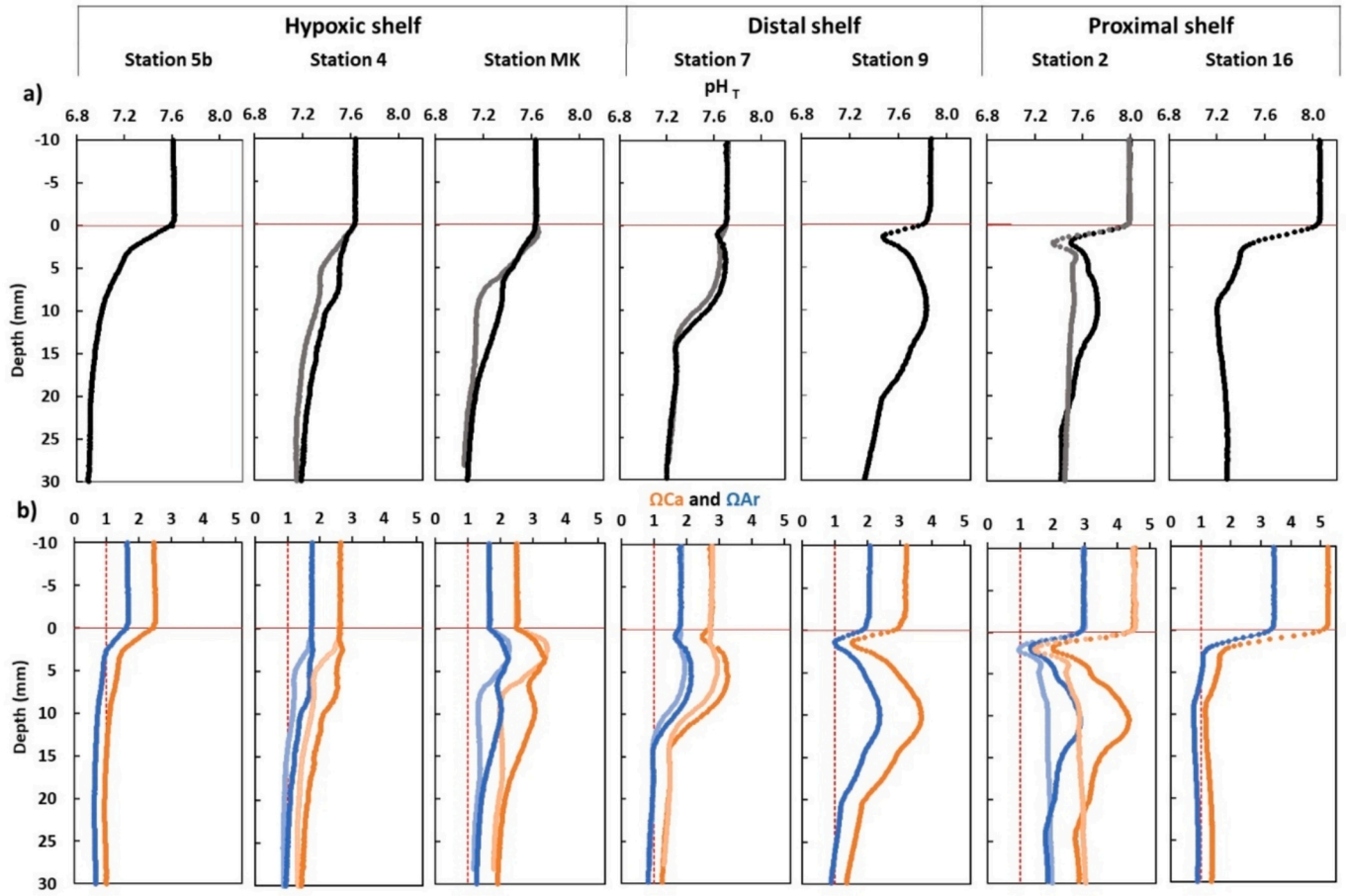

Fig. 5. **(a)** Replicate pH_T microprofiles measured *in situ* at the sediment-water interface on the Louisiana shelf in July 2022**. (b)** Calcium carbonate saturation state with respect to aragonite (blue) and calcite (orange) calculated with pH_T microprofile and interpolated TA profile using the CO2SYS program. The red line indicates the sediment-water interface while the red dashed line represents $\Omega = 1$. (For interpretation of the references to colour in this figure legend, the reader is referred to the web version of this article.)

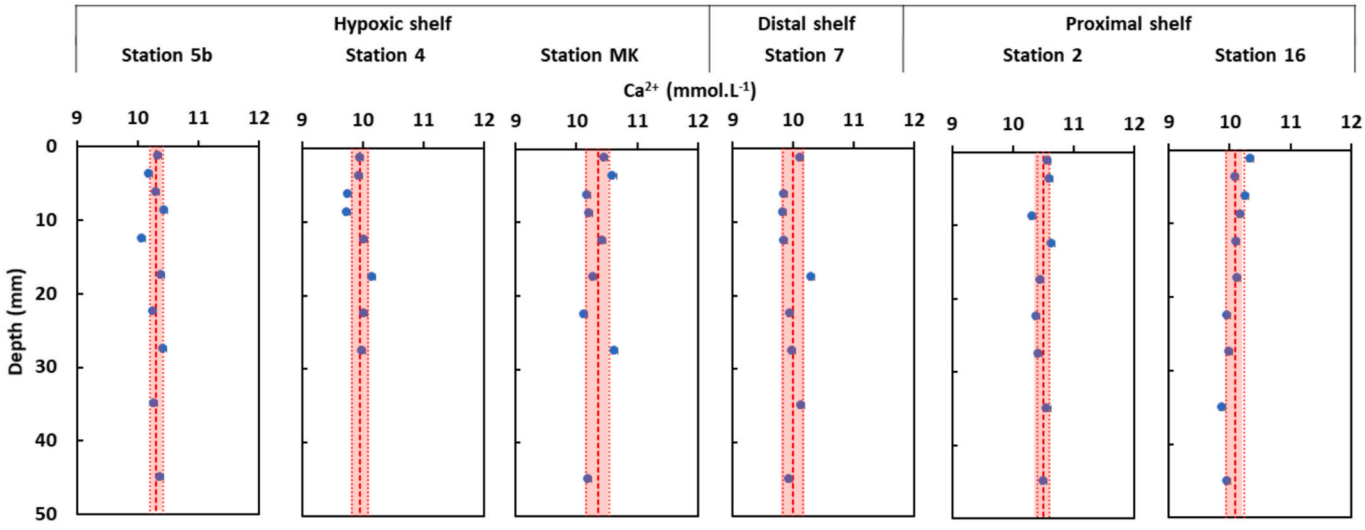

Fig. 6. Vertical distribution of dissolved Ca^{2+} concentration below the sediment-water interface at six stations on the Louisiana shelf in July 2022. Uncertainties are smaller than the symbols size. The dotted red line represents the mean over the whole data set, the shaded part the average standard deviation at each profile. (For interpretation of the references to colour in this figure legend, the reader is referred to the web version of this article.)

DOU rates observed at the proximal shelf stations (Fig. 4). The increase in bottom water temperatures negatively correlated with bottom water O_2 concentrations, as warming boosts the respiration rate of aquatic microorganisms (Hopkinson Jr and E.M, 2005) and reduces O_2 solubility. The large decrease in oxygen concentrations in the bottom waters was coupled with a significant accumulation of DIC (Table 1) and

decrease in pH_T (Fig. 2) resulting from the emission of metabolic CO_2 due to organic matter respiration. The DIC accumulation is partly due to organic matter mineralization in bottom waters but also to DIC flux originating from the sediments (Bianchi et al., 2002; Hu et al., 2017; Berelson et al., 2019; Jiang et al., 2019; Rabouille et al., 2021; Magette et al. *in prep.*).

Consequently, the acidification of bottom water was clearly visible along the east-west transect, with the lowest pH_T values (<7.7) in the most hypoxic areas of the Louisiana shelf. The concomitant decrease in bottom water O_2 concentrations and pH_T displayed a strong linear correlation (Fig. 2, $r^2 > 0.98$), in good agreement with previous studies (Cai et al., 2011; Hu et al., 2017). Considering the two end-member stations of the transect, namely St. 2 in the proximal shelf and St. 5b in the hypoxic area, the differences in pH and oxygen concentrations represent −0.37 pH_T units and − 158 μmol L^{-1}, respectively. In summer 2017, a respective difference of −0.26 pH_T units and − 91 μmol L^{-1} was observed at the same stations (Rabouille et al., 2021). The values are consistent with the previous findings and projections reported by Cai et al. (2011) that benthic acidification ranging from −0.25 to −0.40 pH_T units are expected for a full deoxygenation of the near bottom waters.

4.2. *The biogeochemistry of surficial sediments under strong deoxygenation and acidification*

Along the shelf transect, a comparative analysis of oxygen concentrations in bottom water ($O_{2\text{-BW}}$ Niskin bottle samples collected 1–3 m above the sediment) and in overlying water ($O_{2\text{-OW}}$ *in situ* optode deployed 10–15 cm above the sediment) (Table 1) revealed a strong oxygen gradient in the last few meters of water above the sediment. These marked negative gradients in waters surrounding the sediment support the idea that the sediment oxygen demand partially drives the water column deoxygenation. The differences between $O_{2\text{-BW}}$ and $O_{2\text{-OW}}$ concentrations are most significant at the hypoxic shelf stations (Table 2). These observed gradients support the findings of the summer 2017 (Rabouille et al., 2021), concluding that biogeochemical dynamics at the SWI plays a crucial role in maintaining hypoxic conditions. In the sediment, dissolved oxygen is consumed by oxic degradation of organic matter and oxidation of reduced compounds at the SWI (Glud, 2008). In the absence of any detectable increase in oxygen concentration at the sediment water interface, there is no evidence of benthic primary production in the observed area during the sampling period. As expected, DOUs show a strong relationship with bottom water oxygen concentration (Cai et al., 1995; Glud, 2008). However, the large DOUs calculated in this study for the proximal and distal shelf (Fig. 4) highlight the potential influence of sediment biogeochemical processes on oxygen dynamics, particularly after the deposition of labile organic matter from the Mississippi River nutrients discharges (Laurent et al., 2017). The observed reduction in OPD westward likely reflects reduced oxygen concentration in the overlying water linked to enhanced microbial activity in the bottom waters and the first millimeters of sediment. We assume that bioirrigation did not influence significantly the measured profiles in the hypoxic zone given the absence of characteristic fauna on observation and sieving in the field during Summer 2022 and the preservation of biogeochemical gradients. Organic matter degradation coupled to strong oxygen consumption by aerobic processes therefore represents a key component of the evolution of the bottom waters towards hypoxia (Rabouille et al., 2009).

In the upper thin oxic layer of the sediment, aerobic respiration plays a key role in mineralizing organic matter, producing metabolic CO_2 and H^+ ions in pore waters that significantly decrease the pH_T within the OPD (Cai et al., 1995; Rassmann et al., 2020). Deeper, the oxidation of reduced elements by dissolved O_2 at the oxic-anoxic interface consumes alkalinity, further lowering pH_T (Glud, 2008; Kristensen, 2000; Rassmann et al., 2016), as observed at the proximal shelf stations (Fig. 5). Deeper in the sediment, the relative intensity of biogeochemical processes is evidenced by the significant differences in the asymptotic concentrations of TA and DIC between station 2, which is the most active (13,000 μM), and all other stations (≤ 5000 μM, Fig. 3). These variations in TA and DIC reflect the differing intensities of oxic and anoxic diagenetic processes. Stations closer to the Mississippi River mouth show more intense diagenetic activity at depth (Magette et al., in prep.), resulting in large oxygen consumption and sediment pore water acidification, emphasizing the interconnection between oxygen dynamics, organic matter decomposition, and biogeochemical gradients in the studied area. In the proximal shelf, and to a lesser extent in the distal shelf, deeper in the sediment, the initial decrease in pH_T was followed by a rebound, likely driven by the reduction of metal oxides, which is linked to the anaerobic respiration of OM (Silburn et al., 2017) largely based on metal oxides reduction. Profiles of reduced inorganic species (Mn^{2+}, Fe^{2+}, ΣH_2S, FeS) in sediment pore waters measured during summer 2017 (Rabouille et al., 2021) and summer 2022 (Boever et al., in prep.), showed an accumulation of dissolved Fe^{2+} and Mn^{2+} at intermediate depths (below 3 cm). This accumulation likely explains the observed pH_T pattern, characterized by reduced metal reoxidation near the surface (especially manganese) and metal oxide reduction deeper in the sediment.

In the hypoxic shelf region, the pH_T showed a more monotonic decrease with depth in the sediment in contrast with the pH_T profiles of the proximal stations (Fig. 5). The extent of the pH_T decrease is variable (from −0.4 to −0.7 pH unit) and is certainly linked to anoxic diagenesis and the precipitation of FeS, formed by the combination of accumulated Fe^{2+} during hypoxia with newly produced HS^- from sulfate reduction under anoxic conditions (Mackenzie et al., 1995; Rassmann et al., 2020). The observed spatial and depth patterns align well with the pH_T profiles obtained under similar hypoxic conditions in the summer of 2017 (Rabouille et al., 2021), indicating interannually stable processes under hypoxic conditions.

The biogeochemical reactions involving O_2, pH, DIC, and TA alter the saturation state of bottom waters and sediment pore waters with respect to $CaCO_3$ (Cai and Reimers, 1993; Emerson and Hedges, 2008). All measurements and calculations show that overlying waters exhibit Ω_{Ar} and Ω_{Ca} values above 1, which indicate oversaturation with respect to aragonite and calcite. However, a significant decrease in overlying water Ω_{Ar} and Ω_{Ca} was obvious from east to west along the shelf transect, and the lowest saturation state for both polymorphs was found at station 5b, where hypoxia and acidification conditions are the most intense. Within the sediment, four stations demonstrated undersaturation of pore waters with respect to aragonite, which is 50 % more soluble than calcite (Mucci, 1983). At station 16, where the vertical pH decline in sediment pore waters was most pronounced (≈0.8 pH_T units), the saturation state with respect to aragonite reached $\Omega_{Ar} = 0.7$ at 1 cm below the SWI. In contrast, undersaturation with respect to calcite was not reached in any station except at the most hypoxic station, station 5b. At this station the saturation state reached a critical level in the upper sediment layers, including Ω_{Ar} and Ω_{Ca} of 0.62 and 0.93 (Fig. 5). These undersaturation conditions are thermodynamically favorable for $CaCO_3$ dissolution (Rabouille et al., 2021).

4.3. *The absence of carbonate dissolution during summer hypoxia: hypothesis and implications*

Despite the undersaturation of Ω_{Ar} at four stations on the Louisiana shelf, results from the present study showed no increase in calcium concentrations in the sediment pore waters sampled at the millimeter scale resolution in summer 2022 (Fig. 7). The influence of submarine groundwater discharge can be ruled out as these sediments are identified as silt (Zhang et al., 2023). They are fine, cohesive, non-permeable with consistently high bottom water salinity (>35). As the dissolution of sedimentary carbonate due to the strong acidification of bottom waters would result in increased calcium concentrations, the relatively straight distribution of Ca^{2+} concentration at all stations, including station 5b, clearly indicates the absence of significant $CaCO_3$ dissolution at these

stations.

It is possible to propose an upper bound to carbonate dissolution rates for a given Ca^{2+} gradient. Indeed, at steady-state, the integrated carbonate dissolution rate should equal the Ca^{2+} gradient at the sediment-water interface.

$$D_{s\ Ca}\frac{dCa}{dx} = \int R_{CaCO3}dx \quad (4)$$

where D_{sCa} is the diffusion coefficient for Ca^{2+} in pore waters (4.4 10^{-6} cm^2 sec^{-1}, Li and Gregory, 1974; Berner, 1980), dCa/dx is the calcium gradient in pore waters and $\int R_{CaCO3}dx$ is the integrated rate of carbonate dissolution in the upper sediment.

An increase of 0.5 mmol L^{-1} in the first centimeter which would be detectable, but is absent on our high-resolution profiles (Fig. 6), would result in an integrated rate of carbonate dissolution (*i.e.* flux of calcium) of 1.7 mmol m^{-2} d^{-1}, equivalent to 3.4 mmol m^{-2} d^{-1} of alkalinity. This is clearly much lower than the alkalinity fluxes measured in organic-rich sediments (20–50 mmol m^{-2} d^{-1}; Berelson et al., 2019; Rassmann et al., 2020 and references therein), and indicates that during summer 2022 in the hypoxic sediments, the integrated rate of carbonate dissolution was most probably lower than 1 mmol m^{-2} d^{-1}. Nevertheless, reducing the uncertainties of calcium measurements would allow for a more precise quantification of the underlying diagenetic processes in future studies.

These observations agree with the preliminary work on calcium measurements carried out by Berelson et al. (2019). Although aragonite dissolution appears to be possible at the low bottom water pH of the nGoM, it does not occur to a significant extent under the conditions observed in the summer of 2022. This finding can be explained by the fact that aragonite was not detected by XRD in these relatively low carbonate content sediments (< 10 %), which points towards calcite as the unique stock of calcium carbonate polymorph. The oversaturation with respect to calcite observed in most of these sediments, thus suggest that acidification has to be much more significant to trigger the dissolution of calcite. However, it cannot be completely ruled out that limited amounts of aragonite were deposited with the flux of carbonate and dissolved rapidly in the most hypoxic sediments, thereby leaving an aragonite-free stock of carbonate in the sediments. This is probably not the case at stations 9, 2, and MK where bottom waters and pore waters are oversaturated with respect to aragonite in agreement with the straight Ca^{2+} profiles detected in the upper sediment layers.

The absence of evidence for dissolution at the other stations could also be related to possible inhibition of $CaCO_3$ dissolution by chemical species generated by diagenetic reactions in the sediment pore waters. Several inhibitors, including dissolved organic carbon (DOC, Naviaux et al., 2019) and orthophosphate (Walter and Hanor, 1979), can be adsorbed on the crystal surfaces, protecting $CaCO_3$ from proton or ligand attack and slowing dissolution and precipitation rates. At the investigated stations, DOC concentrations reached an average value of around 375 μmol L^{-1} in the first five centimeters of sediment (Bridgham et al., in prep), levels that are likely high enough to inhibit $CaCO_3$ dissolution. Soluble reactive phosphate and $\sum PO_4^{3-}$ concentrations were also extremely high in the hypoxic shelf during the summer of 2022, which was not observed during sampling in other seasons (Boever et al., in prep; Magette et al., in prep), may also be high enough to inhibit carbonate dissolution. Additionally, dissolved manganese may inhibit carbonate dissolution by forming stable complexes with carbonate, which can stabilize reactive sites on calcite surfaces. Significant Mn(II) concentrations, reaching several hundred μmol L^{-1}, were detected in the sediments of this area during summer 2022 (Boever et al., in prep.), highlighting the important role of the manganese cycle in remineralization of marginal sediments exposed to large riverine inputs (Owings et al., 2021; Rabouille et al., 2021). However, this inhibition is likely reduced in more acidified waters (pH = 7.7), due to the lower stability of these complexes (Vinson et al., 2007). Given the acidified conditions encountered on the Louisiana Shelf, we cannot conclude on the inhibitory effect of Mn(II) on carbonate dissolution.

As the most acidic bottom waters are strongly correlated with hypoxia in summer (Fig. 2; Cai et al., 2011), dissolution of $CaCO_3$ is theoretically less favorable during the rest of the year, under normoxic conditions. However, the abundance of benthic fauna is severely impacted by hypoxia (Burnett and Stickle, 2001), including the *polychaeta* populations on the Louisiana shelf (Rabalais and Baustian, 2020), bioturbation activity resumes during the other seasons and is known to enhance carbonate dissolution in sediment sands (Green and Aller, 2001; Rao et al., 2014). Therefore, bioturbation-driven carbonate dissolution cannot be completely ruled out during other seasons, even when bottom waters are less impacted by acidification and oversaturated.

The absence of $CaCO_3$ dissolution in the nGoM sediments, despite highly acidified and hypoxic bottom water conditions, challenges existing assumptions about carbonate chemistry and the role of shallow carbonate dissolution as a CO_2 sink. Prior to this study, carbonate dissolution at the sediment-water interface in this region had been poorly documented. Although recent researches had provided an overview of benthic processes and fluxes in the nGoM, no definitive conclusions had been drawn regarding carbonate dissolution at the SWI or its contribution to DIC and TA fluxes under summer conditions of hypoxia, acidification, and pore water undersaturation (Berelson et al., 2019; Rabouille et al., 2021; Magette et al., in prep). Recent regional ocean modeling studies, which coupled benthic and pelagic processes for the coastal waters of the nGoM, have assumed that benthic respiration does not involve carbonate dissolution and, therefore, does not contribute to sediment fluxes to the water column (Laurent et al., 2017; Yin et al., 2024). These assumptions were mostly based on observations of bottom water supersaturation. Our sediment-based calculations from the summer of 2022 reinforce this hypothesis, confirming the lack of carbonate dissolution under these conditions. Nevertheless, including the calcium cycle in future models remains crucial for all marine systems, given the significance of carbonate reactions in regulating benthic TA/DIC fluxes and ratio. Projections of intensified coastal acidification due to climate change (Sarmiento and Gruber, 2006; Doney et al., 2007), underscore the importance of this issue for understanding the ocean's response to future environmental stressors (Orr, 2011). Different studies in the Gulf of Saint Lawrence (Nesbitt and Mucci, 2021), in the California Current Ecosytem (Feely et al., 2024), and on carbonate-poor sediments from Catalina Island, California (Lunstrum and Berelson, 2022) provide evidence of dissolution, raising questions about the potential of these sediments as net seawater pH buffers by the middle of the 21st century. In this context, the absence of carbonate dissolution during the hypoxic season in the nGoM, as identified from high-resolution pore water calcium concentrations, suggests a greater stability of calcium carbonate in sediments than previously anticipated. The stability of sedimentary $CaCO_3$ can be integrated into numerical models to avoid overestimating dissolution rates, subsequent alkalinity fluxes, and CO_2 sinks. This study thus provides empirical results that improve our understanding of sedimentary systems in the nGoM and contribute to the future effort in modeling RiOMar systems.

5. Conclusion

This study provides new insights on diagenetic processes in the northern Gulf of Mexico during the July 2022 hypoxic season, with a particular focus on the effect of bottom water acidification on carbonate dissolution. Oxygen concentrations in bottom waters reveal significant spatial variation across the Louisiana Shelf, with strong oxygen depletion at western shelf stations leading to seasonal hypoxia. The large decrease of oxygen concentrations in overlying water is coupled with an accumulation of DIC and a drop in pH, indicating acidification of the bottom waters, by a combination of aerobic respiration and oxidation of reduced metabolites. Sediment biogeochemical processes play a critical role in enhancing oxygen consumption and DIC production, thereby

intensifying hypoxia and acidification of the overlying waters. Despite undersaturation with respect to aragonite and occasionally calcite, dissolved calcium profiles do not show significant dissolution of calcium carbonate minerals. This suggests limited aragonite input or geochemical inhibition of $CaCO_3$ dissolution, potentially influenced by the predominance of calcite as the main carbonate phase and high concentrations of DOC, reactive orthophosphate, and Mn^{2+} in surface sediment pore waters. These findings highlight the importance of incorporating these processes into mathematical models to avoid overestimating dissolution rates and alkalinity fluxes. Simultaneously, the lack of calcium carbonate dissolution in the northern Gulf of Mexico sediments under strong acidified bottom water conditions underscores the stability of calcite in these environments. The data gathered in this study are thus essential to: (i) improve diagenetic models in the nGoM or other eutrophic coastal regions experiencing increased deoxygenation and acidification; (ii) provide critical insights into biogeochemical dynamics at the sediment-water interface; (iii) enhance the accuracy of future acidification projections; and (iv) improve predictions about the future evolution of these ecosystems under the growing pressures of climate change and anthropogenic activities. Understanding these mechanisms is pivotal for refining models of the global carbon cycle and forecasting ecosystem responses to ongoing environmental changes.

CRediT authorship contribution statement

Eva Ferreira: Writing – review & editing, Writing – original draft, Visualization, Validation, Methodology, Investigation, Formal analysis, Data curation, Conceptualization. **Bruno Lansard:** Writing – review & editing, Visualization, Validation, Supervision, Data curation. **Gaël Monvoisin:** Visualization, Methodology, Formal analysis. **Evan Magette:** Writing – review & editing, Visualization, Validation, Investigation. **Anthony Boever:** Writing – review & editing, Visualization, Validation, Investigation. **Hanna Bridgham:** Writing – review & editing, Visualization, Validation, Investigation. **Bruno Bombled:** Methodology, Investigation, Formal analysis. **Jordon Scott Beckler:** Writing – review & editing, Visualization, Validation, Investigation. **Martial Taillefert:** Writing – review & editing, Visualization, Validation, Project administration, Investigation, Funding acquisition. **Christophe Rabouille:** Writing – review & editing, Visualization, Validation, Supervision, Funding acquisition, Data curation.

Acknowledgments

We would like to thank the captain and crew of the R/V Savannah from the Skidaway Institute of Oceanography (University of Georgia) for their support and technical assistance during the operations at sea. We acknowledge Bocar Konte for his help on oxygen profiles processing. DIC and TA measurements in the water column were performed at SNAPO-CO2 at LOCEAN/IPSL (Paris, France). We would like to thank the DIM MAP and the EUR IPSL-Climate Graduate School (project CaPorale), for their financial support, especially for the acquisition of the HPLC for high precision calcium concentration measurements. We would like to thank PANOPLY for their financial support and Amelie Plautre and Julius Nouet for their technical assistance in the carbonate mineral characterization of some of these sediments. This work was funded by the French ANR under the "Investissements d'avenir" program (ANR-11-IDEX-0004-17-EURE-0006) and CNRS International Emerging Actions (AcidHypo). It was also strongly support by the United States NSF Chemical Oceanography (OCE-1948914) and NASA (2020 MUREP OCEAN #4394) programs.

Appendix A. Appendix

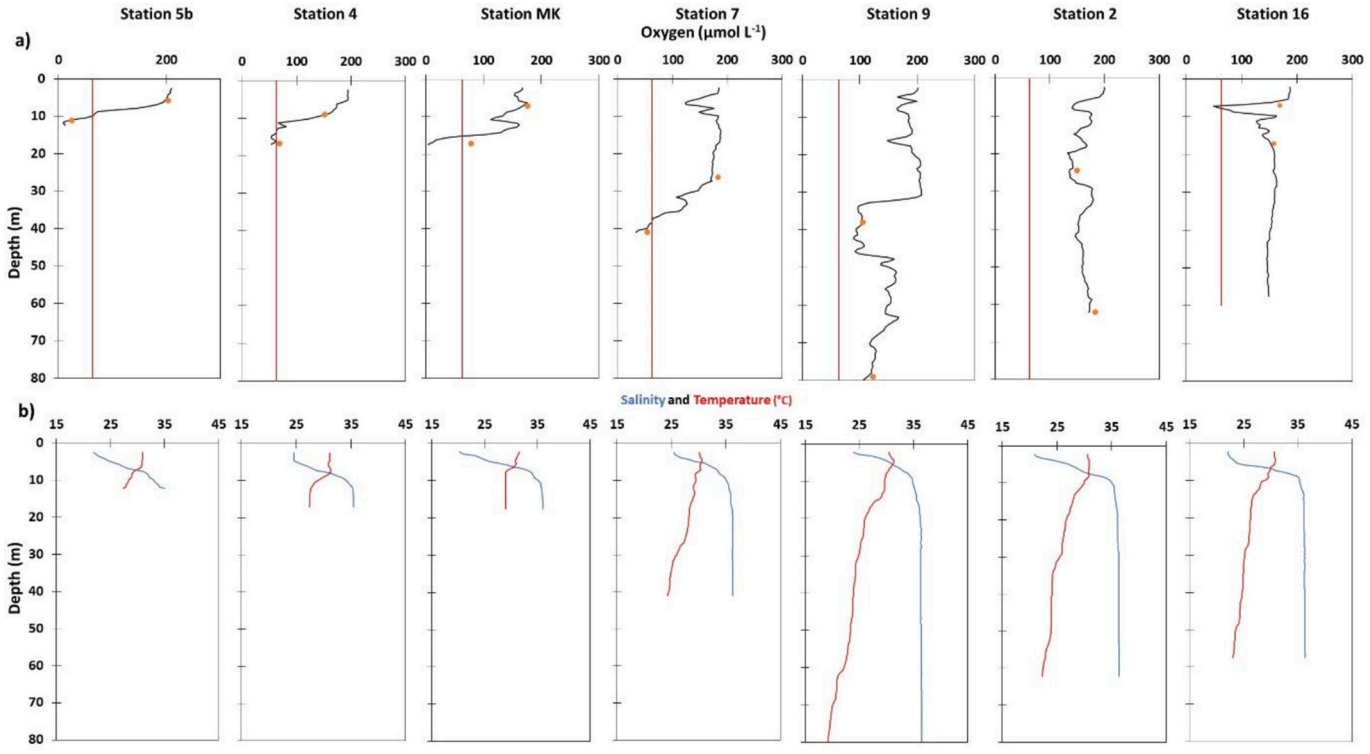

Appendix 1. (a) Vertical Oxygen profile in the water column (µmol.L^{-1},black), the red line corresponds to the hypoxia threshold and the orange dots to the Winkler measurements. (b) Temperature (°C, red) and salinity (blue) profiles in the water column at six stations on the Louisiana shelf in July 2022.

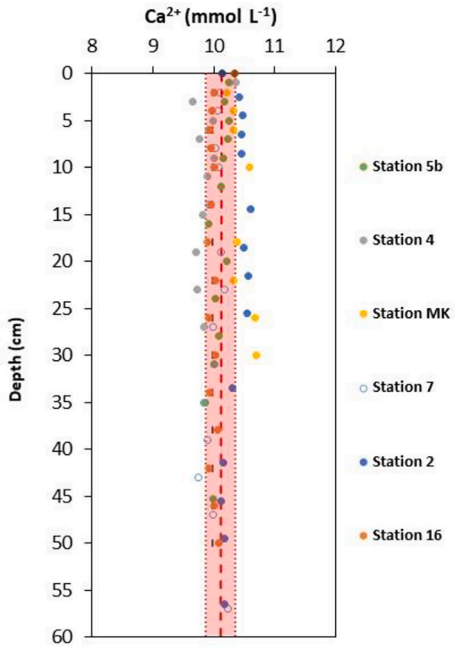

Appendix 2. Vertical distribution of dissolved Ca2+ concentration in the sediment at six stations on the Louisiana shelf in July 2022. Uncertainties are smaller than the symbols size. The dotted red line represents the mean over the whole data set, the shaded part the average standard deviation.

Data availability

All data used in this study are available through SEANOE (doi:10.17882/102870, Ferreira et al., 2024).

References

Balsam, W.L., Beeson, J.P., 2003. Sea-floor sediment distribution in the Gulf of Mexico. Deep-Sea Res. I Oceanogr. Res. Pap. 50 (12), 1421–1444. https://doi.org/10.1016/j.dsr.2003.06.001.

Bauer, J.E., Cai, W.J., Raymond, P.A., Bianchi, T.S., Hopkinson, C.S., Regnier, P.A., 2013. The changing carbon cycle of the coastal ocean. Nature 504 (7478), 61–70. https://doi.org/10.1038/nature12857.

Berelson, W.M., McManus, J., Severmann, S., Rollins, N., 2019. Benthic fluxes from hypoxia-influenced Gulf of Mexico sediments: impact on bottom water acidification. Mar. Chem. 209, 94–106. https://doi.org/10.1016/j.marchem.2019.01.004.

Berner, R.A., 1980. Early Diagenesis: A Theoretical Approach. Princeton University Press, New Jersey.

Bianchi, T.S., Mitra, S., McKee, B.A., 2002. Sources of terrestrially-derived organic carbon in lower Mississippi River and Louisiana shelf sediments: implications for differential sedimentation and transport at the coastal margin. Mar. Chem. 77 (2), 211–223. https://doi.org/10.1016/S0304-4203(01)00088-3.

Bianchi, T.S., Galler, J.J., Allison, M.A., 2007. Hydrodynamic sorting and transport of terrestrially derived organic carbon in sediments of the Mississippi and Atchafalaya Rivers. Estuar. Coast. Shelf Sci. 73 (1), 211–222. https://doi.org/10.1016/j.ecss.2007.01.004.

Bianchi, T.S., DiMarco, S.F., Cowan, J.H., Hetland, R.D., Chapman, P., Day, J.W., Allison, M.A., 2010. The science of hypoxia in the northern Gulf of Mexico: a review. Sci. Total Environ. 408 (7), 1471–1484. https://doi.org/10.1016/j.scitotenv.2009.11.047.

Boudreau, B.P., Jorgensen, B.B., 2001. The Benthic boundary layer: transport processes and biogeochemistry. Oxford University Press, Oxford.

Breitburg, D., Levin, L.A., Oschlies, A., Grégoire, M., Chavez, F.P., Conley, D.J., Garçon, V., Gilbert, D., Gutiérrez, D., Isensee, K., Jacinto, G.S., Limburg, K.E., Montes, I., Naqvi, S.W.A., Pitcher, G.C., Rabalais, N.N., Roman, M.R., Rose, K.A., Seibel, B.A., Telszewski, M., Yasuhara, M., Zhang, J., 2018. Declining oxygen in the global ocean and coastal waters. Science 359 (6371), eaam7240. https://doi.org/10.1126/science.aam7240.

Burnett, L.E., Stickle, W.B., 2001. Physiological responses to hypoxia. In: Rabalais, Nancy N., Eugene Turner, R. (Eds.), Coastal Hypoxia: Consequences for Living Resources and Ecosystems. Coastal and Estuarine Studies 58. American Geophysical Union, Washington, D.C., pp. 101–114

Byrne, M., Fitzer, S., 2019. The impact of environmental acidification on the microstructure and mechanical integrity of marine invertebrate skeletons. Conserv. Physiol 7 (1), coz062. https://doi.org/10.1093/conphys/coz062.

Cai, W.J., Reimers, C.E., 1993. The development of pH and pCO_2, microelectrodes for studying the carbonate chemistry of pore waters near the sediment-water interface. Limnol. Oceanogr. 38 (8), 1762–1773. https://doi.org/10.4319/lo.1993.38.8.1762.

Cai, W.-J., Reimers, C.E., Shaw, T., 1995. Microelectrode studies of organic carbon degradation and calcite dissolution at a California continental rise site. Geochim. Cosmochim. Acta 59 (3), 497–511. https://doi.org/10.1016/0016-7037(95)00316-R.

Cai, W.-J., Hu, X., Huang, W.-J., Murrell, M.C., Lehrter, J.C., Lohrenz, S.E., Chou, W.C., Zhai, W., Hollibaugh, J.T., Wang, Y., Zhao, P., Guo, X., Gundersen, K., Dai, M., Gong, G.-C., 2011. Acidification of subsurface coastal waters enhanced by eutrophication. Nat. Geosci. 4 (11), 766–770. https://doi.org/10.1038/ngeo1297.

Cai, W.-J., Feely, R.A., Testa, J.M., Li, M., Evans, W., Alin, S.R., Xu, Y.-Y., Pelletier, G., Ahmed, A., Greeley, D.J., Newton, J.A., Bednaršek, N., 2021. Natural and anthropogenic drivers of acidification in large estuaries. Annu. Rev. Mar. Sci. 13, 23–55. https://doi.org/10.1146/annurev-marine-010419-011004.

Clayton, T.D., Byrne, R.H., 1993. Spectrophotometric seawater pH measurements: total hydrogen ion concentration scale calibration of m-cresol purple and at-sea results. Deep-Sea Res. I Oceanogr. Res. Pap. 40 (10), 2115–2129. https://doi.org/10.1016/0967-0637(93)90048-8.

Dai, M., Su, J., Zhao, Y., Hofmann, E.E., Cao, Z., Cai, W.-J., Gan, J., Lacroix, F., Laruelle, G.G., Meng, F., Müller, J.D., Regnier, P.A.G., Wang, G., Wang, Z., 2022. Carbon fluxes in the Coastal Ocean: synthesis, boundary processes, and future trends. Annu. Rev. Earth Planet. Sci. 50 (Volume 50, 2022), 593–626. https://doi.org/10.1146/annurev-earth-032320-090746.

Deng, X., Li, Q., Su, J., Liu, C.-Y., Atekwana, E., Cai, W.-J., 2022. Performance evaluations and applications of a δ13C-DIC analyzer in seawater and estuarine waters. Sci. Total Environ. 833, 155013. https://doi.org/10.1016/j.scitotenv.2022.155013.

Dickson, A.G., 1990. Thermodynamics of the dissociation of boric acid in synthetic seawater from 273.15 to 318.15 K. Deep Sea Research Part A. Oceanographic Research Papers 37 (5), 755–766. https://doi.org/10.1016/0198-0149(90)90004-F.

Dickson, A.G., Sabine, C.L., Christian, J.R., 2007. Guide to best practices for ocean CO_2 measurement. In: PICES special publication 3, 8. IOCCP Report, p. 191. https://doi.org/10.25607/OBP-1342.

Doney, S.C., 2010. The growing human footprint on coastal and open-ocean biogeochemistry. Science 328 (5985), 1512–1516. https://doi.org/10.1126/science.1185198.

DOE, 1994. In: Dickson, A.G., Goyet, C. (Eds.), Handbook of methods for the analysis of the various parameters of the carbon dioxide system in sea water; version 2. https://doi.org/10.2172/10107773.

Doney, S.C., Mahowald, N., Lima, I., Feely, R.A., Mackenzie, F.T., Lamarque, J.-F., Rasch, P.J., 2007. Impact of anthropogenic atmospheric nitrogen and sulfur deposition on ocean acidification and the inorganic carbon system. Proc. Natl. Acad. Sci. 104 (37), 14580–14585. https://doi.org/10.1073/pnas.0702218104.

Doney, S.C., Fabry, V.J., Feely, R.A., Kleypas, J.A., 2009. Ocean acidification: the other CO2 problem. Annu. Rev. Mar. Sci. 1, 169–192. https://doi.org/10.1146/annurev.marine.010908.163834.

Doney, S.C., Busch, D.S., Cooley, S.R., Kroeker, K.J., 2020. The impacts of ocean acidification on marine ecosystems and reliant human communities. Annu. Rev.

Environ. Resour. 45, 83–112. https://doi.org/10.1146/annurev-environ-012320-083019.
Dortch, Q., Rabalais, N.N., Turner, R.E., Rowe, G.T., 1994. Respiration rates and hypoxia on the Louisiana shelf. Estuaries 17 (4), 862–872. https://doi.org/10.2307/1352754.
Emerson, S.R., Hedges, J.I., 2008. Chemical Oceanography and the Marine Carbon Cycle. Cambridge University Press, pp. 101–130. https://doi.org/10.1017/CBO9780511793202.
Feely, R.A., Carter, B.R., Alin, S.R., Greeley, D., Bednaršek, N., 2024. The combined effects of ocean acidification and respiration on habitat suitability for marine Calcifiers along the west coast of North America. J. Geophys. Res. Oceans 129 (4), e2023JC019892. https://doi.org/10.1029/2023JC019892.
Fennel, K., Testa, J.M., 2019. Biogeochemical controls on coastal hypoxia. Annu. Rev. Mar. Sci. 11 (Volume 11, 2019), 105–130. https://doi.org/10.1146/annurev-marine-010318-095138.
Glud, R.N., 2008. Oxygen dynamics of marine sediments. Mar. Biol. Res. 4 (4), 243–289. https://doi.org/10.1080/17451000801888726.
Green, M.A., Aller, Robert C., 2001. Early diagenesis of calcium carbonate in Long Island sound sediments: benthic fluxes of Ca2+ and minor elements during seasonal periods of net dissolution. J. Mar. Res. 59 (5). https://doi.org/10.1357/002224001762674935.
Hansen, H.P., 1999. Determination of oxygen. In: Grasshoff, K.K. Klaus, Ehrhardt, Manfred (Eds.), Methods of Seawater Analysis, pp. 75–89.
He, H., Li, Y., Wang, S., Ma, Q., Pan, Y., 2020. A high precision method for calcium determination in seawater using ion chromatography. Front. Mar. Sci. 7, 231. https://doi.org/10.3389/fmars.2020.00231.
Hopkinson Jr., C.S.S., E.M, 2005. Estuarine respiration: An overview of benthic, pelagic and whole system respiration. In: del Giorgio, P., Williams, P. (Eds.), Respiration in Aquatic Ecosystems. Oxford University Press, pp. 122–146.
Hu, X., Cai, W.-J., 2011. An assessment of ocean margin anaerobic processes on oceanic alkalinity budget. Glob. Biogeochem. Cycles 25 (3). https://doi.org/10.1029/2010GB003859.
Hu, X., Li, Q., Huang, W.-J., Chen, B., Cai, W.-J., Rabalais, N.N., Eugene, T.R., 2017. Effects of eutrophication and benthic respiration on water column carbonate chemistry in a traditional hypoxic zone in the northern Gulf of Mexico. Mar. Chem. 194, 33–42. https://doi.org/10.1016/j.marchem.2017.04.004.
Jahnke, R.A., Jahnke, D.B., 2004. Calcium carbonate dissolution in deep sea sediments: reconciling microelectrode, pore water and benthic flux chamber results. Geochim. Cosmochim. Acta 68 (1), 47–59. https://doi.org/10.1016/S0016-7037(03)00260-6.
Jiang, Z.-P., et al., 2019. Physical and biogeochemical controls on pH dynamics in the northern Gulf of Mexico during summer hypoxia. J. Geophys. Res. Oceans 124 (8), 5979–5998. https://doi.org/10.1029/2019JC015140.
Kristensen, E., 2000. Organic matter diagenesis at the oxic/anoxic interface in coastal marine sediments, with emphasis on the role of burrowing animals. Hydrobiologia 426 (1), 1–24. https://doi.org/10.1023/A:1003980226194.
Krumins, V., Gehlen, M., Arndt, S., Van Cappellen, P., Regnier, P., 2013. Dissolved inorganic carbon and alkalinity fluxes from coastal marine sediments: model estimates for different shelf environments and sensitivity to global change. Biogeosciences 10 (1), 371–398. https://doi.org/10.5194/bg-10-371-2013.
Laurent, A., Fennel, K., Wilson, R., Lehrter, J., Devereux, R., 2016. Parameterization of biogeochemical sediment–water fluxes using in situ measurements and a diagenetic model. Biogeosciences 13 (1), 77–94. https://doi.org/10.5194/bg-13-77-2016.
Laurent, A., Fennel, K., Cai, W.-J., Huang, W.-J., Barbero, L., Wanninkhof, R., 2017. Eutrophication-induced acidification of coastal waters in the northern Gulf of Mexico: insights into origin and processes from a coupled physical-biogeochemical model. Geophys. Res. Lett. 44 (2), 946–956. https://doi.org/10.1002/2016GL071881.
Li, Y.H., Gregory, S., 1974. Diffusion of ions in sea water and in deep-sea sediments. Geochim. Cosmochim. Acta 38 (5), 703–714. https://doi.org/10.1016/0016-7037(74)90145-8.
Liu, X., Patsavas, M.C., Byrne, R.H., 2011. Purification and characterization of meta-cresol purple for spectrophotometric seawater pH measurements. Environ. Sci. Technol. 45 (11), 4862–4868. https://doi.org/10.1021/es200665d.
Lueker, T.J., Dickson, A.G., Keeling, C.D., 2000. Ocean pCO_2 calculated from dissolved inorganic carbon, alkalinity, and equations for K1 and K2: validation based on laboratory measurements of CO_2 in gas and seawater at equilibrium. Mar. Chem. 70 (1), 105–119. https://doi.org/10.1016/S0304-4203(00)00022-0.
Lunstrum, A., Berelson, W., 2022. CaCO3 dissolution in carbonate-poor shelf sands increases with ocean acidification and porewater residence time. Geochim. Cosmochim. Acta 329, 168–184. https://doi.org/10.1016/j.gca.2022.04.031.
Mackenzie, F.T., Vink, S., Wollast, R., Chou, L., 1995. Comparative geochemistry of marine Saline Lakes. In: Lerman, A., Imboden, D.M., Gat, J.R. (Eds.), Physics and Chemistry of Lakes. Springer, Berlin Heidelberg, Berlin, Heidelberg, pp. 265–278.
McKee, B.A., Aller, R.C., Allison, M.A., Bianchi, T.S., Kineke, G.C., 2004. Transport and transformation of dissolved and particulate materials on continental margins influenced by major rivers: benthic boundary layer and seabed processes. Cont. Shelf Res. 24 (7–8), 899–926. https://doi.org/10.1016/j.csr.2004.02.009.
Metzl, N., et al., 2024. An updated synthesis of ocean total alkalinity and dissolved inorganic carbon measurements from 1993 to 2023: the SNAPO-CO2-v2 dataset. Earth Syst. Sci. Data Discuss. 2024, 1–39. https://doi.org/10.5194/essd-2024-464.
Mucci, A., 1983. The solubility of calcite and aragonite in seawater at various salinities, temperatures, and one atmosphere total pressure. Am. J. Sci. 283 (7), 780–799. https://doi.org/10.2475/ajs.283.7.780.
Mucci, A., Sundby, B., Gehlen, M., Arakaki, T., Zhong, S., Silverberg, N., 2000. The fate of carbon in continental shelf sediments of eastern Canada: a case study. Deep-Sea Res. II Top. Stud. Oceanogr. 47 (3–4), 733–760. https://doi.org/10.1016/S0967-0645(99)00124-1.
Murray, C.N., Riley, J.P., 1969. The solubility of gases in distilled water and sea water—II. Oxygen. Deep Sea Res. Oceanogr. Abstr. 16 (3), 311–320. https://doi.org/10.1016/0011-7471(69)90021-7.
Naviaux, J.D., Subhas, A.V., Dong, S., Rollins, N.E., Liu, X., Byrne, R.H., Berelson, W.M., Adkins, J.F., 2019. Calcite dissolution rates in seawater: lab vs. in-situ measurements and inhibition by organic matter. Mar. Chem. 215, 103684. https://doi.org/10.1016/j.marchem.2019.103684.
Nesbitt, W.A., Mucci, A., 2021. Direct evidence of sediment carbonate dissolution in response to bottom-water acidification in the Gulf of St. Lawrence, Canada. Can. J. Earth Sci. 58 (1), 84–92. https://doi.org/10.1139/cjes-2020-0020.
NOAA National Centers for Environmental Information, 2023. Coastal Relief Models (CRMs) [dataset]. crm_vol3_2023, crm_vol4_2023. https://doi.org/10.25921/5ZN5-KN44.
Orr, J.C., 2011. In: Gattuso, A.L.H. Jean-Pierre (Ed.), Recent and future changes in ocean carbonate chemistry. Ocean acidification, Oxford, pp. 41–66.
Orr, J.C., Epitalon, J.M., Gattuso, J.-P., 2015. Comparison of ten packages that compute ocean carbonate chemistry. Biogeosciences 12 (5), 1483–1510. https://doi.org/10.5194/bg-12-1483-2015.
Owings, S.M., Bréthous, L., Eitel, E.M., Fields, B.P., Boever, A., Beckler, J.S., Bombled, B., Lansard, B., Metzger, E., Rabouille, C., Taillefert, M., 2021. Differential manganese and iron recycling and transport in continental margin sediments of the northern Gulf of Mexico. Mar. Chem. 229. https://doi.org/10.1016/j.marchem.2020.103908.
Paerl, H.W., 2006. Assessing and managing nutrient-enhanced eutrophication in estuarine and coastal waters: interactive effects of human and climatic perturbations. Ecol. Eng. 26, 40–54. https://doi.org/10.1016/j.ecoleng.2005.09.006.
Pierrot, D., Lewis, E., Wallace, D.W.R., 2006. MS Excel program developed for CO_2 system calculations., ORNL/CDIAC-105a. Carbon Dioxide Information Analysis Center, Oak Ridge National Laboratory, U.S. Department of Energy, Tennessee. Carbon Dioxide Information Analysis Center, Oak Ridge National Laboratory, U.S. Department of Energy, Oak Ridge, Tennessee.
Rabalais, N.N., 2022. Report from 2022 shelf-Wide Hypoxia Cruise. https://www.hpc.msstate.edu/NewsEvents/docs/2022/Hypoxia_editedpressrelease8-2-22.pdf.
Rabalais, N.N., Baustian, M.M., 2020. Historical shifts in benthic Infaunal diversity in the northern Gulf of Mexico since the appearance of seasonally severe hypoxia. Diversity 12 (2). https://doi.org/10.3390/d12020049.
Rabalais, N.N., Turner, R.E., 2001. Hypoxia in the Northern Gulf of Mexico: Description, Causes and Change, Coastal Hypoxia: Consequences for Living Resources and Ecosystems, pp. 1–36.
Rabalais, N.N., Turner, R.E., 2019. Gulf of Mexico hypoxia: past, present, and future. Limnolo. Oceanogr. Bull. 28 (4). https://doi.org/10.1002/lob.10351.
Rabalais, N.N., Turner, R.E., Wiseman, W.J., 2002. Gulf of Mexico hypoxia, a.k.a. "the dead zone". Annu. Rev. Ecol. Syst. 33, 235–263. https://doi.org/10.1146/annurev.ecolsys.33.010802.150513.
Rabalais, N.N.C.W.-J., Jacob, Carstensen, Conley Daniel, J., Brian, Fry, Xinping, Hu, Zoraida, Quiñones-Rivera, Rutger, Rosenberg, Slomp Caroline, P., Eugene, Turner R., Maren, Voss, Björn, Wissel, Jing, Zhang, 2014. Eutrophication-driven deoxygenation in the Coastal Ocean. Oceanography 27, 172–183. https://doi.org/10.5670/oceanog.2014.21.
Rabouille, C., Gaillard, J.F., 1991. A coupled model representing the deep-sea organic carbon mineralization and oxygen consumption in surficial sediments. J. Geophys. Res. 96 (C2), 2761–2776. https://doi.org/10.1029/90JC02332.
Rabouille, C., Caprais, J.C., Lansard, B., Crassous, P., Dedieu, K., Reyss, J.L., Khripounoff, A., 2009. Organic matter budget in the Southeast Atlantic continental margin close to the Congo canyon: in situ measurements of sediment oxygen consumption. Deep-Sea Res. II Top. Stud. Oceanogr. 56 (23), 2223–2238. https://doi.org/10.1016/j.dsr2.2009.04.005.
Rabouille, C., Lansard, B., Owings, S., Rabalais, N.N., Bombled, B., Metzger, E., Richirt, J., Eitel, E., Boever, A., Beckler, J., Taillefert, M., 2021. Early diagenesis in the hypoxic and acidified zone of the northern Gulf of Mexico: is organic matter recycling in sediments disconnected from the water column? Front. Mar. Sci. 8, 604330. https://doi.org/10.3389/fmars.2021.604330.
Rao, A.M.F., Malkin, S.Y., Montserrat, F., Meysman, F.J.R., 2014. Alkalinity production in intertidal sands intensified by lugworm bioirrigation. Estuar. Coast. Shelf Sci. 148, 36–47. https://doi.org/10.1016/j.ecss.2014.06.006.
Rassmann, J., Lansard, B., Pozzato, L., Rabouille, C., 2016. Carbonate chemistry in sediment porewaters of the Rhône River delta driven by early diagenesis (northwestern Mediterranean). Biogeosciences 13 (18), 5379–5394. https://doi.org/10.5194/bg-13-5379-2016.
Rassmann, J., Eitel, E.M., Lansard, B., Cathalot, C., Brandily, C., Taillefert, M., Rabouille, C., 2020. Benthic alkalinity and dissolved inorganic carbon fluxes in the Rhône River prodelta generated by decoupled aerobic and anaerobic processes. Biogeosciences 17 (1), 13–33. https://doi.org/10.5194/bg-17-13-2020.
Redalje, D.G., Fahnenstiel, G.L., 1994. The relationship between primary production and the vertical export of particulate organic matter in a river-impacted coastal ecosystem. Estuaries 17 (4), 829–838. https://doi.org/10.2307/1352751.
Revsbech, N.P., 1989. An oxygen microsensor with a guard cathode. Limnol. Oceanogr. 34 (2), 474–478. https://doi.org/10.4319/lo.1989.34.2.0474.
Sarmiento, J.L., Gruber, N., 2006. *Ocean Biogeochemical Dynamics*. Princeton University Press. https://doi.org/10.2307/j.ctt3fgxqx.
Silburn, B., Kröger, S., Parker, E.R., Sivyer, D.B., Hicks, N., Powell, C.F., Johnson, M., Greenwood, N., 2017. Benthic pH gradients across a range of shelf sea sediment types linked to sediment characteristics and seasonal variability. Biogeochemistry 135 (1), 69–88. https://doi.org/10.1007/s10533-017-0323-z.

Turner, R.E., Rabalais, N.N., Justic, D., 2008. Gulf of Mexico hypoxia: alternate states and a legacy. Environ. Sci. Technol. 42 (7), 2323–2327. https://doi.org/10.1021/es071617k.

Uppström, L.R., 1974. The boron/chlorinity ratio of deep-sea water from the Pacific Ocean. Deep-Sea Res. and Oceanogr. 21, 161–162. https://doi.org/10.1016/0011-7471(74)90074-6.

Vinson, M.D., Arvidson, R.S., Luttge, A., 2007. Kinetic inhibition of calcite (104) dissolution by aqueous manganese(II). J. Cryst. Growth 307 (1), 116–125. https://doi.org/10.1016/j.jcrysgro.2007.05.059.

Wallace, R.B., Baumann, H., Grear, J.S., Aller, R.C., Gobler, C.J., 2014. Coastal Ocean acidification: the other eutrophication problem. Estuar. Coast. Shelf Sci. 148, 1–13. https://doi.org/10.1016/j.ecss.2014.05.027.

Walter, L.M., Hanor, J.S., 1979. Effect of orthophosphate on the dissolution kinetics of biogenic magnesian calcites. Geochim. Cosmochim. Acta 43 (8), 1377–1385. https://doi.org/10.1016/0016-7037(79)90128-5.

Wang, H., Hu, X., Rabalais, N.N., Brandes, J., 2018. Drivers of oxygen consumption in the northern Gulf of Mexico hypoxic waters—a stable carbon isotope perspective. Geophys. Res. Lett. 45 (19), 10,528–10,538. https://doi.org/10.1029/2018GL078571.

Yin, D., Cui, L., Harris, C.K., Moriarty, J.M., Beck, H., Maiti, K., 2024. The role of benthic fluxes in acidifying the bottom waters in the northern Gulf of Mexico hypoxic zone based on an updated water column biogeochemical-seabed diagenetic and sediment transport model. J. Adv. Model. Earth Syst. 16 (10), e2023MS004045. https://doi.org/10.1029/2023MS004045.

Zhang, W., et al., 2023. Spatial and temporal variations of seabed sediment characteristics in the inner Louisiana shelf. Mar. Geol. 463, 107115. https://doi.org/10.1016/j.margeo.2023.107115.